PNAS RESEARCH ARTICLE | ENVIRONMENTAL SCIENCES

Synthetic DNA fragments as ultra-high-resolution multitracers to quantify transport behavior of micro- and nanoplastics in plant systems

Zhaofei Duan[a,1], Changxi Wang[a,1], Renkuan Liao[a,2], Yanling Liao[a], Xinlin Li[a], Chongyang Shen[a], Yunwu Xiong[b], Dayong Yang[c], Jirka Šimůnek[d], and Dan Luo[e]

Affiliations are included on p. 11.

Edited by Catherine J. Murphy, University of Illinois Urbana-Champaign, Urbana, IL; received February 11, 2026; accepted July 31, 2026

Although plant uptake of micro- and nanoplastics (MNPs) has been well documented, accurately identifying MNP sources and tracking their transport within plants remain major challenges, primarily due to the lack of effective multisource tracing technologies. To fill this gap, we established an ultra-high-resolution multisource tracing approach by encapsulating sequence-specific synthetic DNA fragments into MNPs, followed by quantification of their transport using quantitative real-time PCR (qPCR) in controlled lettuce cultivation experiments. This approach enables the quantification of source-specific MNP contributions in plants, while providing quantitative evidence for size-dependent transport behavior and the involvement of transpiration in MNP uptake. High transpiration (VPD = 2.12 kPa) resulted in 10-fold and 20-fold elevations in the MNP bioconcentration factor (BCF) and translocation factor (TF) of lettuce, respectively, compared with low transpiration (VPD = 0.34 kPa). Size-dependent accumulation of MNPs was observed: 200 nm particles exhibited higher BCF and greater TF than 700 nm particles. Smaller particles were preferentially translocated to shoots, while larger ones were retained in roots. Irrigation represented the predominant pathway of MNP uptake (BCF = 1.5×10^{-2}), showing higher accumulation than both the atmosphere (BCF = 2.2×10^{-3}) and the substrate (BCF = 4.9×10^{-4}). The observed patterns also support that atmospherically deposited MNPs penetrate plant tissues through leaf stomata. The findings validate the effectiveness of the synthetic DNA-based labeling approach, providing critical quantitative data to advance our understanding of interaction mechanisms between MNPs and plants.

DNA tracers | emerging pollutants | lettuce uptake | particulate | biomarker

Significance

Quantifying the source- and size-dependent transport contributions of micro- and nanoplastics (MNPs) in plants has been challenging. We address this limitation by developing an ultra-high-resolution synthetic DNA-based multisource tracing technology that quantifies plant MNP sources and their size-dependent translocation dynamics. Our findings provide quantitative evidence supporting the role of plant transpiration as a major physiological driver of MNP bioaccumulation. Particle size determines where MNPs accumulate across plant organs, with smaller MNPs exhibiting enhanced translocation to above-ground tissues. Our study identifies irrigation as the primary route through which MNPs invade plants, in contrast to atmosphere and substrate pathways. This work fills the gap in quantitative methodologies for assessing MNP risks in plants and demonstrates synthetic DNA labeling as a powerful tool.

Plastics, synthetic materials primarily composed of high-molecular-weight polymers such as polyethylene (PE), polypropylene (PP), polystyrene (PS), and polylactic acid (PLA), are broadly deployed across packaging, construction, healthcare, and electronics by virtue of their low cost, light weight, corrosion resistance, and favorable processability (1–3). Plastic debris is categorized by size into macroplastics (>5 mm), microplastics (0.1 μm to 5 mm), and nanoplastics (<0.1 μm) (4). Of these fractions, micro- and nanoplastics (MNPs) have emerged as a pervasive global environmental concern. Their small particle size, large specific surface area, and high chemical stability allow long-term persistence and mobility across multiple environmental compartments, including water, soil, atmosphere, and vegetation (5, 6). In terrestrial ecosystems, agricultural soils are experiencing progressive MNP accumulation, driven primarily by residual mulch films, wastewater irrigation, atmospheric deposition, and the application of plastic-contaminated organic fertilizers (7, 8). Although the environmental risks caused by conventional PE, PP, and PS MNPs have been extensively investigated (9–13), growing evidence indicates that biodegradable PLA MNPs also pose substantial ecological risks (14–16). Recent work has shown that PLA MNPs exert stronger alterations in arsenic fractionation and microbial communities than PE MNPs, raising a potentially greater threat to ecological safety (17). These findings underscore that MNPs represent a highly persistent and multifaceted global threat that compromises both environmental sustainability and public health.

Studies have demonstrated that plants can uptake and accumulate MNPs through multiple pathways. Pioneering work by Li et al. (18) provided the first direct visual evidence, using fluorescence labeling, that wheat and lettuce roots absorb polystyrene (PS) and polymethyl methacrylate (PMMA) MNPs through cracks generated during lateral root growth, after which they were further distributed throughout the plant via the transpiration stream. In a pivotal study, the uptake of PS MNPs with different surface

The authors declare no competing interest.

This article is a PNAS Direct Submission.

Copyright © 2026 the Author(s). Published by PNAS. This article is distributed under Creative Commons Attribution-NonCommercial-NoDerivatives License 4.0 (CC BY-NC-ND).

[1]Z.D. and C.W. contributed equally to this work.

[2]To whom correspondence may be addressed. Email: renkuanliao@163.com.

This article contains supporting information online at https://www.pnas.org/lookup/suppl/doi:10.1073/pnas.2605150123/-/DCSupplemental.

Published August 27, 2026.

Downloaded from https://www.pnas.org by CHINA AGRICULTURAL UNIVERSITY on August 27, 2026 from IP address 202.112.160.48.

charges in *Arabidopsis thaliana* has been investigated using a combined fluorescence and palladium labeling approach (19). Their results demonstrated distinct pathways: negatively charged PS MNPs predominantly entered through the apoplastic route and accumulated in root vasculature, whereas positively charged PS MNPs aggregated on the root surface and root hairs due to interactions with root exudates, resulting in limited internal transport. The first detection of MNPs in cucumbers was subsequently reported using pyrolysis gas chromatography-mass spectrometry (Py-GC/MS), showing that PS MNPs translocate from roots to stems and leaves over time (20). Subsequently, fluorescence-labeling assays of wheat roots further suggested that the Casparian strip and cell wall act as barriers to particle uptake, allowing PS MNPs smaller than 40 nm to penetrate into the cytoplasm, while largely restricting the entry of particles larger than 100 nm (21). In the same year, a novel dual-functional probe based on europium chelates was developed to integrate fluorescence imaging with inductively coupled plasma mass spectrometry (ICP-MS), enabling quantitative tracking of low-dose MNPs (22). Subsequent improvements of this labeling technique enabled in situ detection of MNPs within plant tissues (23). The results showed that PS MNPs ranging from 30 nm to 2 μm can directly penetrate maize leaves through stomata and translocate into the mesophyll and vascular bundles, with higher uptake efficiency as leaves aged and stomatal conductance increased. These findings extend our understanding of MNP entry pathways, covering not only root uptake but also foliar absorption. Transpiration, particle size, and surface charge are considered major factors regulating MNP uptake and translocation in plants (18, 21). While fluorescence and europium chelate labeling are effective for quantifying plant MNP uptake (18, 20, 23), these techniques are restricted by the limited variety of available labeling markers and endogenous plant fluorescence interference. Such drawbacks hinder the development of abundant high-resolution tracers, which are indispensable for characterizing the dynamic transport of MNPs under complex scenarios—such as when MNPs of different sources and sizes coexist within plant tissues.

The recent emergence of high-resolution tracing technology based on synthetic DNA fragments has created new opportunities for the specific labeling of particulate matter, such as silica, clay, PLA, and iron oxide (24–27). In this approach, uniquely sequenced DNA fragments are encapsulated into target particles to act as tracers, which enables their subsequent high-sensitivity detection via qPCR (28–30). For example, the first synthetic DNA-labeled PLA nanoparticles incorporating paramagnetic iron oxide were synthesized via a double emulsion method through the encapsulation of unique 200-base-pair DNA fragments; their scalable tracing capability systematically verified across column, plot, and stream scales (31). Paunescu et al. (25) proposed an electrostatic adsorption-mediated sol–gel method for encapsulating double- and single-stranded DNA fragments, genomic DNA, and plasmids within silica layers, thereby developing the first DNA-labeled silica nanoparticles. Subsequently, the synthetic DNA labeling technique has been gradually extended to real-world applications in quantifying the drift rate and range of pesticide particles, characterizing glacial flow pathways, identifying septic system pollution sources and differentiating the transport behavior of colloids with varying particle sizes in porous media (26, 32–34). Collectively, synthetic DNA fragments offer three core advantages: precise nanoscale controllability, excellent biocompatibility, and environmental friendliness. Leveraging these merits, they can theoretically generate an unlimited number of unique sequences through base-pair combinations and label target substances without introducing contamination. Each DNA sequence functions as a distinctive tracer that can be detected with high sensitivity using qPCR, thereby providing a vast library of specific markers to support multisource tracing applications.

This study aimed to develop an ultra-high-resolution multisource tracing framework via encapsulation of sequence-specific DNA fragments into MNPs. The specific objectives were to i) quantify the uptake, translocation, and in-plant distribution of MNPs under varying transpiration conditions; ii) evaluate the relative contributions of multiple MNP sizes (200 nm and 700 nm) and sources, including substrate, atmosphere, and irrigation; and iii) elucidate the fundamental mechanisms governing MNP uptake and transport in plants. Lettuce (*Lactuca sativa* L.), a widely cultivated and consumed vegetable crop, was selected as the test plant for controlled hydroponic and sand culture experiments. Biodegradable poly(lactic-co-glycolic acid) (PLGA) was used to fabricate MNPs in this study. Multiple 80-bp synthetic DNA fragments were designed for specific labeling of MNPs derived from three environmental sources (substrate, atmosphere, and irrigation) and two particle sizes (200 and 700 nm). The concentrations of these DNA-labeled MNPs were ultimately quantified using a standard curve established between qPCR signal intensities and MNP concentration. The findings can provide critical insights into the interaction mechanisms between MNPs and plants.

1. Results

1.1. Fabrication and Characterization of DNA-Labeled MNPs.

1.1.1. Particle size control of DNA-labeled MNPs. The DNA-labeled MNPs were fabricated using the double-emulsion method, as illustrated in Fig. 1*A*. The particle size of the resultant DNA-labeled MNPs was significantly affected by three key preparation parameters: substance PLGA concentrations, ultrasonic power levels, and emulsifier concentrations. Particle size was positively correlated with PLGA concentration (Fig. 1*B*). Specifically, when the PLGA concentration increased from 5 to 15%, the average particle size increased from 248.6 ± 12.9 to 589.2 ± 41.9 nm ($P \leq 0.001$). Higher PLGA concentrations elevate solution viscosity, which weakens the ultrasound shearing effect and facilitates particle aggregation during solvent evaporation, ultimately leading to the formation of larger particles (35, 36). A negative correlation was observed between particle size and ultrasonic power (Fig. 1*C*). As the power increased from 25 to 175 W, the average particle size decreased from 532.3 ± 50.8 to 227.3 ± 13.1 nm ($P \leq 0.001$). High-frequency ultrasound causes cavitation at the oil–water interface, producing microjets that break down emulsion droplets. In contrast, low-power conditions provide insufficient energy, resulting in droplet coalescence (37, 38). Similarly, the particle size exhibited a negative correlation with the concentration of the emulsifier (Fig. 1*D*). As the emulsifier concentration increased from 0.05 to 0.7%, the average particle size decreased from 596.5 ± 42.8 to 270.0 ± 7.9 nm ($P \leq 0.001$). Emulsifiers form a protective layer at the oil–water interface, enhancing particle hydrophilicity and preventing aggregation. Higher concentrations reduce interfacial tension, yielding smaller and more stable droplets during ultrasonication (39). Above the emulsifier concentration of 0.5%, particle size stabilizes, indicating saturation of the emulsifier effect. The zeta potential of DNA-labeled MNPs remained stable (−29 to −46 mV) across all tested conditions, indicating that the experimental parameters had minimal impact on surface charge. The consistent negative potential is attributed to PLGA carboxyl groups, confirming that process conditions affect particle formation rather than surface chemistry.

Downloaded from https://www.pnas.org by CHINA AGRICULTURAL UNIVERSITY on August 27, 2026 from IP address 202.112.160.48.

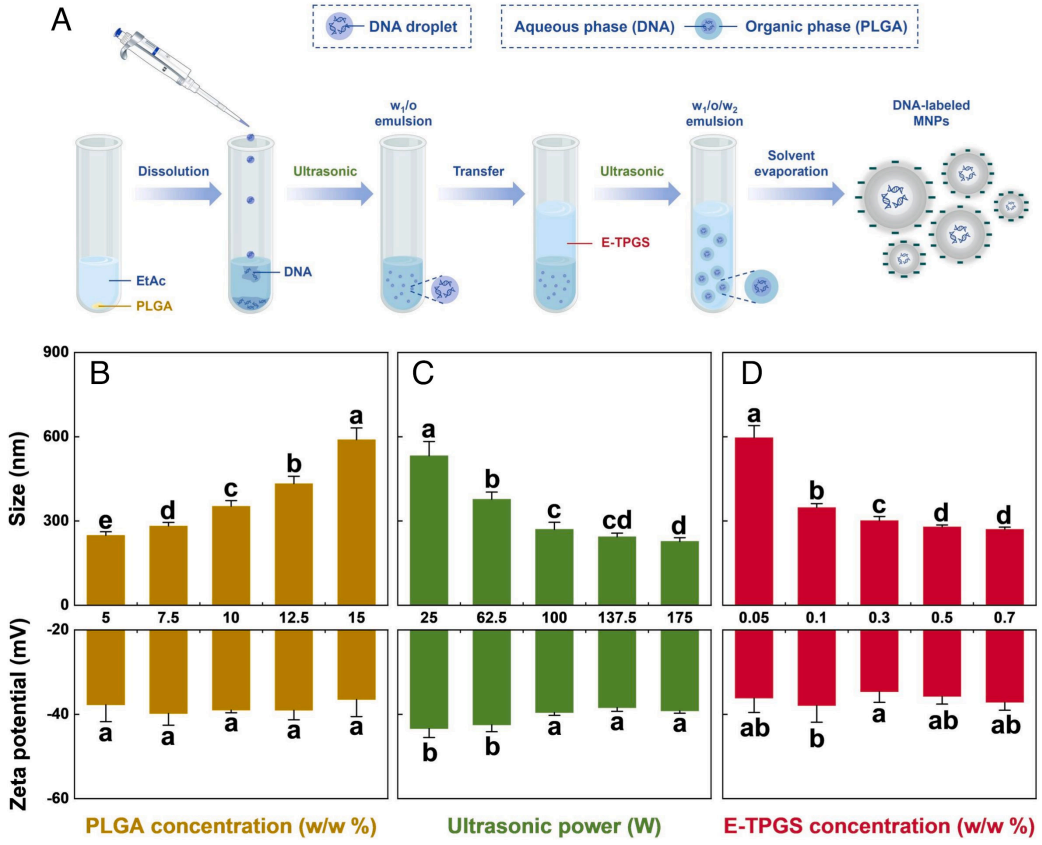

Fig. 1. Fabrication and characterization of DNA-labeled PLGA (DNA-PLGA) MNPs. (*A*) Schematic illustration of the fabrication of DNA-PLGA MNPs via the double emulsion method. Particle size and zeta potential of DNA-PLGA MNPs under different (*B*) substance PLGA concentrations, (*C*) ultrasonic power, and (*D*) emulsifier vitamin E-TPGS concentrations. Error bars indicate SD, and data are shown as mean ± SD based on nine independent measurements ($n = 9$). Different lowercase letters indicate significant differences among different fabrication conditions for each parameter, as determined by one-way ANOVA followed by Duncan's multiple range test ($P \leq 0.05$, $n = 9$).

1.1.2. Characterization of the physicochemical properties of DNA-labeled MNPs. DNA-labeled MNPs with average sizes of 200 nm (0.7% E-TPGS concentration, 175 W ultrasonic power, 10% PLGA concentration, labeled by DNA2) and 700 nm (0.1% E-TPGS concentration, 100 W ultrasonic power, 15% PLGA concentration, labeled by DNA3), along with unlabeled MNPs, were fabricated in this study. FTIR spectroscopic analysis (*SI Appendix*, Fig. S1*A*) showed that both labeled and unlabeled MNPs displayed typical PLGA characteristic peaks at approximately 1,761 cm^{-1} (C=O stretching), 1,180 to 1,275 cm^{-1} (C–O–C/C–O stretching), and 2,880 to 2,999/1,394 to 1,456 cm^{-1} (C–H stretching). The consistent spectral profiles verified that DNA encapsulation did not alter the surface chemical properties of the PLGA. Minor absorbance enhancements observed at 1,090 to 1,130 cm^{-1} were likely attributed to the vibrational modes of DNA phosphate groups and nucleobases, while the overall spectral features remained consistent with pristine PLGA. These results suggest that DNA encapsulation exerts negligible effects on the surface chemical properties of MNPs, with the weak characteristic signals primarily originating from surface-adsorbed DNA fragments.

Scanning electron microscopy (SEM) observations demonstrated that both 200 nm and 700 nm DNA-labeled MNPs were spherical or near-spherical with smooth surfaces (*SI Appendix*, Fig. S1 *B* and *C*). While most MNPs were well within the designed size range, sporadic size outliers were also observed. This particle size heterogeneity likely arose from heterogeneous shear forces caused by localized ultrasonic energy gradient during the two-step emulsification process. During the solvent evaporation, inhomogeneous temperature and solute concentration caused differential solvent removal rates. Certain low-viscosity oil droplets tended to grow further via Ostwald ripening or coalescence, a typical phenomenon for particles synthesized using double emulsion methods (39, 40). Dynamic light scattering (DLS) results further indicated that the hydrodynamic diameter of 200 nm MNPs ranged from 135.9 to 254.4 nm (with a predominant distribution between 84.9 and 407.2 nm), whereas the 700 nm particles exhibited sizes of 557.2 to 1043.2 nm. A small fraction of oversized particles (up to 3 to 4 μm) was also detected (*SI Appendix*, Fig. S1 *D* and *E*). Zeta potential measurements confirmed that all MNPs possessed highly negative surface charges, averaging −39.2 ± 0.9 mV for the 200 nm group and −43.1 ± 2.6 mV for the 700 nm group.

PCR amplification coupled with agarose gel electrophoresis verified the specific binding and amplification of the five synthetic DNA sequences by their respective primer pairs, and no evident cross-amplification was observed for mismatched primer pairs (*SI Appendix*, Fig. S2). Strong linear correlations ($R^2 > 0.98$) were observed between the concentrations of the five types of DNA-labeled MNPs and their corresponding qPCR Cq values (*SI Appendix*, Fig. S3), confirming the accurate conversion of qPCR signals into MNP mass. DNA encapsulation and extraction efficiencies were greater than 95% and 84%, respectively (*SI Appendix*, Table S1). Stability assays in Hoagland solution showed stable DNA concentrations (200 nm: 0.8 to 1.7 × 10^{-6} μM; 700 nm: 0.4 to 0.7 × 10^{-6} μM) across shaking periods of 1 to 6 d, with no significant difference from control groups ($P > 0.05$, *SI Appendix*, Table S2). These results demonstrate the excellent structural stability of

Downloaded from https://www.pnas.org by CHINA AGRICULTURAL UNIVERSITY on August 27, 2026 from IP address 202.112.160.48.

DNA-labeled MNPs and the negligible release of DNA, validating their feasibility for long-term cultivation experiments.

1.2. Transpiration-Driven Uptake and Translocation of MNPs in Lettuce. Analysis of MNP abundance in lettuce roots, stems, and leaves at 10 and 30 d after transplantation indicated that transpiration pull acts as a critical regulator governing MNP uptake and translocation. Under high transpiration conditions (VPD = 2.12 kPa), substantial MNP accumulation was observed in all plant tissues. In contrast, MNP uptake was markedly restricted under low transpiration conditions (VPD = 0.34 kPa). A pronounced difference was observed on day 10: robust MNP accumulation occurred in the high transpiration group, whereas net MNP uptake was undetectable in all tissues of the low transpiration group (Fig. 2*A*). Statistical analysis confirmed these disparities were extremely significant in stems and leaves ($P \leq 0.001$) and significant in roots ($P \leq 0.05$). By day 30, although marginal MNP uptake was detected in the roots and stems under low transpiration conditions, upward translocation to aerial tissues remained constrained, with no net MNP accumulation observed in leaves (Fig. 2*B*). Consequently, significant differences in MNP accumulation were evident in all tissues between the two transpiration treatments, with the strongest difference observed in roots ($P \leq 0.001$), followed by leaves ($P \leq 0.01$) and stems ($P \leq 0.05$). These findings demonstrate that elevated transpiration pull substantially accelerates the net uptake and upward translocation of MNPs throughout the growth period.

Further analysis of MNP accumulation levels, bioconcentration factor (BCF), translocation factor (TF), and distribution patterns indicated distinct behaviors under different transpiration conditions. Under high transpiration conditions, MNP accumulation and translocation were rapid and efficient. On day 10, the plants exhibited a high total MNP load of 2.8 μg plant^{-1} (BCF = 1.1 × 10^{-4}) and a TF of 38.2, reflecting intense MNP uptake and predominant accumulation in leaves. By day 30, total MNP accumulation increased sharply to 31.0 μg plant^{-1} (BCF = 4.1 × 10^{-4}), but the TF decreased to 4.7, suggesting a shift toward more even tissue distribution, although leaves still served as the primary MNP sink (Fig. 2*C*). Under low transpiration conditions, uptake was delayed and limited. No MNPs were detected at day 10 (BCF = 0). By day 30, only low accumulation (3.0 μg plant^{-1}; BCF = 4.0 × 10^{-5}) and a very low TF (0.2) were recorded. These results reflect inefficient translocation: MNPs were confined to roots and stems, with no particles transported to leaves (Fig. 2*D*).

SEM observations confirmed the uptake of MNPs in lettuce (Fig. 3). No particles were observed in either roots or leaves of the MNP-free control groups. In contrast, distinct particles were clearly visible in both root epidermis and mesophyll cell walls of the treated plants, demonstrating successful uptake and translocation of MNPs. Notably, the morphology of the PLGA-based MNPs in the SEM images may differ from their pristine state due to the material's inherent thermal sensitivity. As a biodegradable polymer susceptible to thermal deformation at temperatures above 120 °C, PLGA particles may soften, fuse, or aggregate under the localized heat generated by gold-sputtering or prolonged electron beam exposure (41, 42). Such thermal artifact accounted for the irregular particle shapes or apparent clustering observed in the images.

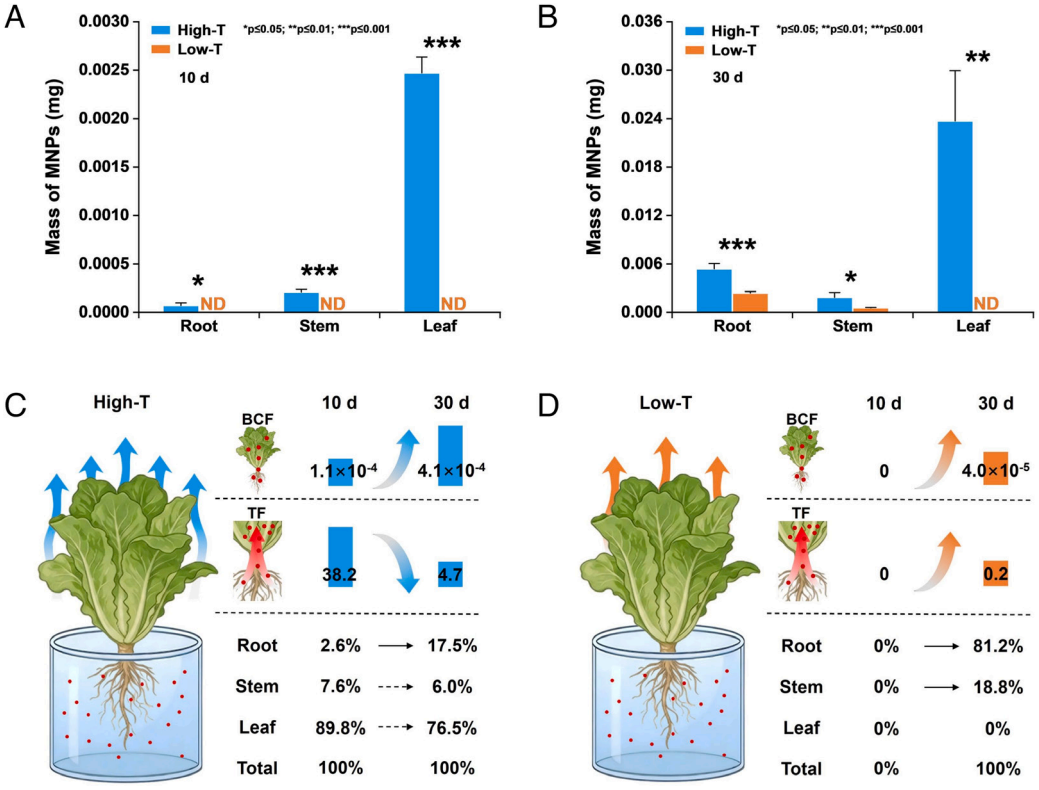

Fig. 2. Impacts of transpiration pull on MNP uptake, translocation, and distribution in lettuce. Net MNP accumulation in lettuce roots, stems, and leaves under high transpiration (High-T) and low transpiration (Low-T) conditions at (*A*) day 10 and (*B*) day 30. Temporal variations in the bioconcentration factor (BCF; the ratio of MNP mass in whole lettuce seedlings to the initial MNP mass of the exposure medium), translocation factor (TF; the ratio of MNP mass in aerial tissues to root tissues), and proportional tissue distribution (%) of MNPs under (*C*) High-T and (*D*) Low-T conditions. Solid and dashed arrows indicate increased and decreased MNP proportional distribution, respectively. Error bars indicate SD, and data are shown as mean ± SD based on three independent biological replicates ($n = 3$). Significant differences between High-T and Low-T groups were determined using independent-samples *t* tests ($n = 3$). *$P \leq 0.05$; **$P \leq 0.01$; ***$P \leq 0.001$. ND indicates nondetectable.

Downloaded from https://www.pnas.org by CHINA AGRICULTURAL UNIVERSITY on August 27, 2026 from IP address 202.112.160.48.

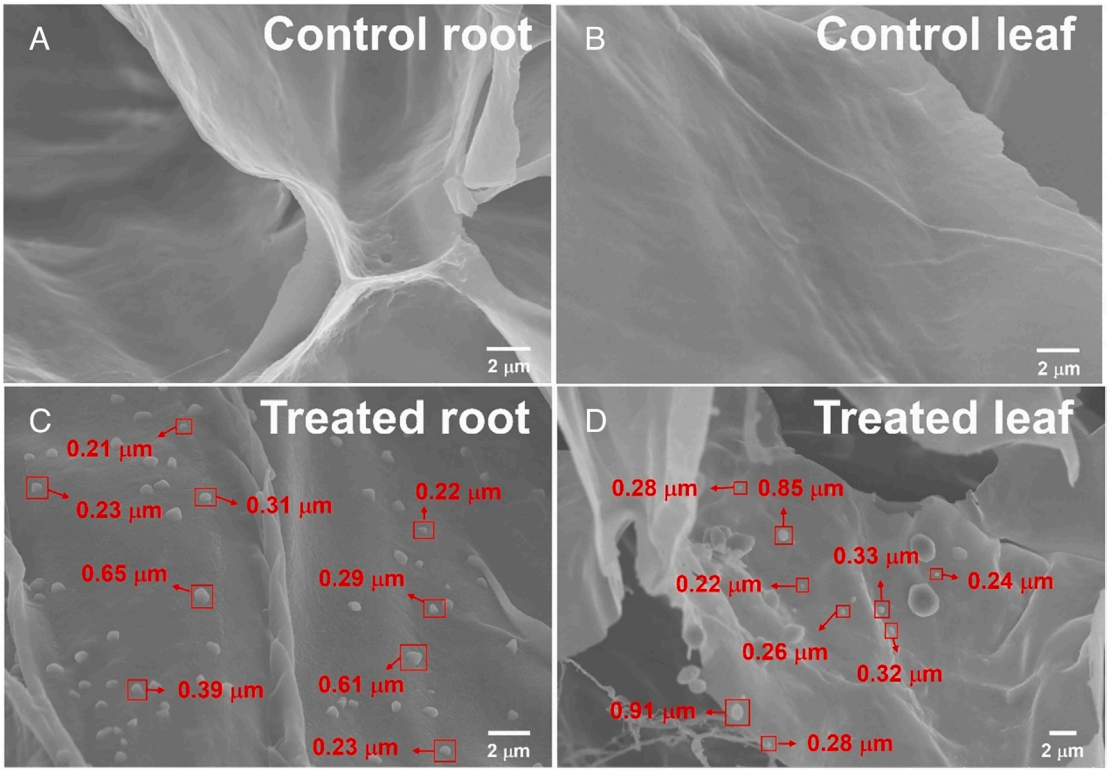

Fig. 3. SEM observations of MNP distribution in lettuce tissues under high transpiration conditions on day 30 posttransplantation. (*A* and *B*) MNP-free control groups for root and leaf. (*C* and *D*) MNP-exposed groups for root and leaf. Root and leaf refer to root epidermis and mesophyll cell walls, respectively.

1.3. Size-Dependent Uptake and Translocation of MNPs in Lettuce. Analysis of net MNP accumulation in lettuce tissues at days 10 and 30 revealed obvious size-dependent differences in uptake and translocation. Across the entire experimental period, 200 nm MNPs exhibited persistently higher uptake efficiency than their 700 nm counterparts. On day 10, this size-driven disparity was particularly prominent across the whole plant, with significant differences were observed in roots and leaves ($P \le 0.01$) and in stems ($P \le 0.05$), indicating that the smaller 200 nm particles more readily overcame physical barriers during initial entry and acropetal transport (Fig. 4*A*). The preferential accumulation of smaller particles persisted until day 30. At this time point, the difference in net accumulation between the two particle sizes remained extremely significant in the stem ($P \le 0.001$) and highly significant in the roots and leaves ($P \le 0.01$) (Fig. 4*B*). These results demonstrate that smaller particle size serves as a critical factor enhancing the bioavailability and upward translocation of MNPs in the plant tissues.

Further analysis of MNP accumulation, BCF, and TF revealed significant size-dependent differences. The 200 nm MNPs showed robust uptake (0.2 mg plant^{-1} on day 10; 1.3 mg plant^{-1} on day 30) and higher BCF values (1.2×10^{-2} to 1.5×10^{-2}), while 700 nm MNPs were absorbed less effectively (1.6 and 16.8 μg plant^{-1}; BCF = 8.2×10^{-5} and 1.9×10^{-4}) (Fig. 4*C*). Although both particle sizes were initially transported to leaves, 200 nm MNPs achieved a more uniform distribution over time, with their TF declining from 12.3 to 2.9. In contrast, 700 nm MNPs were predominantly retained in roots, with TF values of 5.2 and 0.8 at the two sampling time points, indicative of severely restricted upward mobility (Fig. 4*D*). The consistently higher BCF and TF values of 200 nm MNPs demonstrate that smaller particles possess superior absorption and translocation efficiency in plants.

SEM observations further confirmed MNP uptake in the sand-cultured lettuce, with no particles detected in the MNP-free control tissues (Fig. 5). For MNP-exposed plants, both 200 and 700 nm particles were observed in the roots, with the smaller particles being far more abundant. Leaves were predominantly colonized by 200 nm particles, whereas larger particles were only sporadically detected. These findings indicate that the smaller MNPs feature higher uptake efficiently and greater mobility for translocation to aboveground tissues, which corroborates the size-dependent uptake and translocation trends quantified by qPCR.

1.4. Comparative Uptake and Translocation of MNPs from Different Sources in Lettuce. Comparative analysis of net MNP accumulation from three exposure pathways—substrate, atmosphere, and irrigation water—revealed pronounced source-dependent differences in uptake efficiency. Irrigation acted as the predominant route for MNP uptake across all plant tissues and sampling time points. On day 10, MNP accumulation in both roots and stems followed the order: irrigation > atmosphere > substrate (Fig. 6*A*). In these two tissues, MNP accumulation from irrigation was significantly or highly significantly greater than that from the atmosphere and substrate pathways, whereas no significant difference was observed between the atmosphere and substrate sources. Leaves exhibited a distinct distribution pattern at this early stage, ranked as irrigation > substrate > atmosphere with highly significant differences among all three exposure pathways ($P \le 0.01$). By day 30, the predominance of irrigation-derived MNP uptake persisted, with the accumulation profile stabilizing to a consistent order of irrigation > atmosphere > substrate across all tissues (Fig. 6*B*). Statistical analysis showed that, across roots, stems, and leaves, MNP accumulation from irrigation was significantly higher ($P \le 0.01$) than that from the atmosphere and substrate pathways.

Downloaded from https://www.pnas.org by CHINA AGRICULTURAL UNIVERSITY on August 27, 2026 from IP address 202.112.160.48.

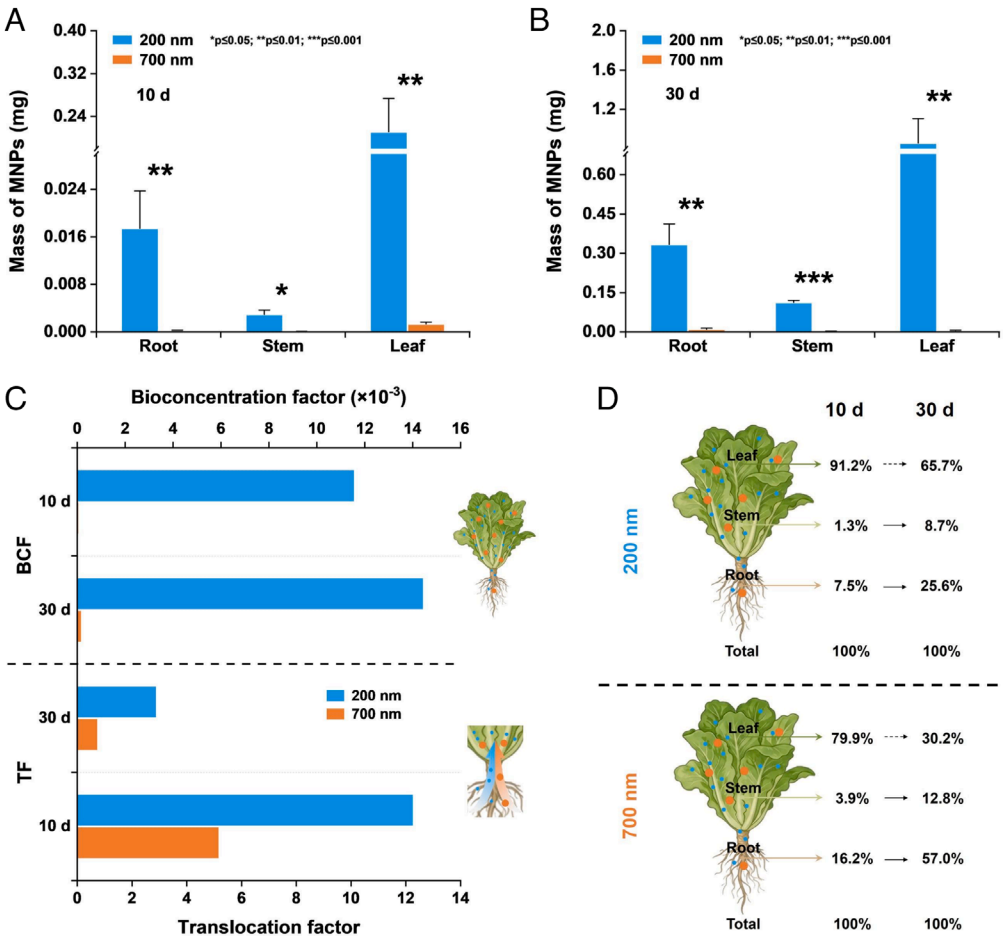

Fig. 4. Size-dependent uptake and translocation of MNPs in lettuce. Net MNP accumulation in lettuce roots, stems, and leaves for 200 and 700 nm MNPs at (*A*) day 10 and (*B*) day 30. (*C*) BCF (the ratio of MNP mass in whole lettuce seedlings to the initial MNP mass of the exposure medium) and TF (the ratio of MNP mass in aerial tissues to root tissues) of the two MNP sizes on days 10 and 30. (*D*) Temporal variations in the relative MNP distribution proportions (%) in lettuce roots, stems, and leaves for both MNP sizes. Solid and dashed arrows indicate increased and decreased MNP proportional distribution, respectively. Error bars indicate SD, and data are shown as mean ± SD based on three independent biological replicates (n = 3). Significant differences between MNP sizes were determined using independent-samples t tests (n = 3). *$P \le 0.05$; **$P \le 0.01$; ***$P \le 0.001$.

In contrast, no significant difference was observed between the atmosphere and substrate sources in any tissue. These results indicate that irrigation represented the dominant exposure pathway, whereas MNP accumulation from atmospheric deposition and substrate-derived exposure was comparable under the tested conditions.

Further analysis of MNP accumulation, BCF, and TF revealed source-dependent uptake disparities. MNPs originating from irrigation exhibited the highest uptake and accumulation in lettuce, followed by those from atmosphere, while substrate-derived MNPs showed the lowest uptake efficiency. On day 10, BCF values followed the order: irrigation (BCF = 1.2×10^{-2}) > atmosphere (BCF = 2.1×10^{-4}) > substrate (BCF = 7.4×10^{-5}). By day 30, MNP accumulation increased across all three exposure pathways, with irrigation remaining the highest (BCF = 1.5×10^{-2}), followed by atmosphere (BCF = 2.2×10^{-3}), and substrate (BCF = 4.9×10^{-4}) (Fig. 6*C*). Notably, the BCF of atmospheric-derived MNPs rose by 10.1-fold, a markedly greater increase than those of the substrate (6.6-fold) and irrigation (1.3-fold) groups. This pronounced increase was accompanied by a distinct tissue-distribution pattern: although the relative proportion of MNPs in leaves decreased over time for all three exposure pathways, the decline was much smaller in the atmosphere group (3.5%) than in the substrate (19.0%) and irrigation (25.5%) groups (Fig. 6*D*). Together, these results suggest that atmospherically deposited MNPs may have been retained to a greater extent in leaf tissues during the later exposure stage, potentially because the expanded leaf areas and developed surface structures, enhancing particle deposition and stomatal uptake (23). Accordingly, the traditional root-to-shoot TF was not calculated for this group, as the primary entry route was not restricted to the root system.

In contrast, MNP originating from the substrate and irrigation followed a typical root-to-shoot translocation pattern that gradually reached equilibrium. Both groups showed high initial TF on day 10 (Substrate: 33.5, Irrigation: 12.3), corresponding to predominant MNP accumulation in the leaves. However, by day 30, TF values decreased markedly (Substrate: 6.7, Irrigation: 2.9). This decline in translocation efficiency aligned perfectly with the tissue distribution results, where the relative proportion of MNPs in the leaves decreased over time (Fig. 6 *C* and *D*). Collectively, these findings indicate that while rapid upward transport takes place at the early stage, MNPs eventually distribute more evenly across roots, stems, and leaves as lettuce grows.

2. Discussion

We successfully established and validated a synthetic DNA labeling—qPCR approach for tracing and quantifying the dynamics of MNPs within plants. By designing unique DNA fragments for labeling MNPs of different sizes (200 and 700 nm) and sources (substrate, atmosphere, and irrigation), we achieved quantitative tracking of the

Downloaded from https://www.pnas.org by CHINA AGRICULTURAL UNIVERSITY on August 27, 2026 from IP address 202.112.160.48.

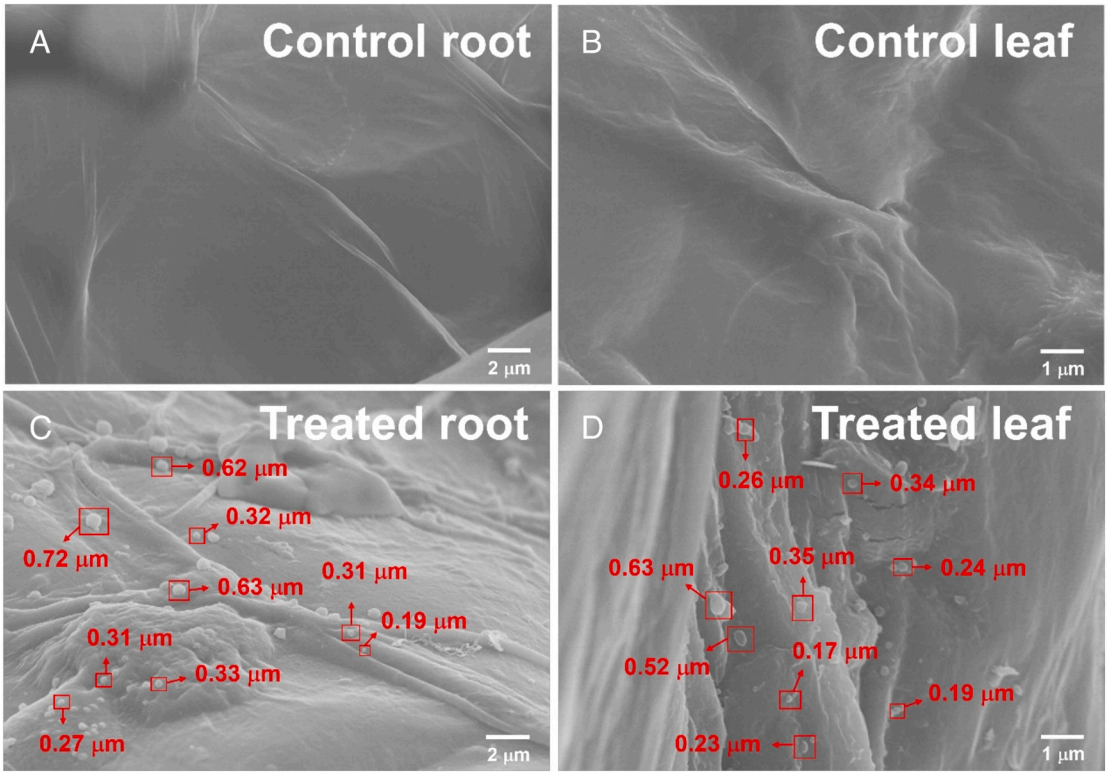

Fig. 5. SEM observations of 200 nm and 700 nm MNP distribution in lettuce tissues on day 30 posttransplantation. (*A* and *B*) MNP-free control groups for root and leaf. (*C* and *D*) MNP-exposed groups for root and leaf. Root and leaf refer to root epidermis and mesophyll cell walls, respectively.

uptake, translocation, and fate of MNPs in lettuce. This approach addresses the drawbacks of existing labeling techniques, such as fluorescence-based methods (which suffer from plant autofluorescence interference) or metal-based tracers (which are limited in applicable marker diversity) (22, 43), enabling unambiguous differentiation of MNPs under complex exposure scenarios. It provides a high-resolution tool to deepen our knowledge of plant–MNP interactions.

In this study, biodegradable PLGA was selected as the experimental MNP primarily stems from two considerations. On the one hand, although biodegradable MNPs are generally considered more environmentally benign than nonbiodegradable MNPs (44, 45), their degradation products or related polyester-based plastics have been reported to exert phytotoxic effects on soybean, rice, and maize, including inhibited root development, and reduced biomass accumulation (15, 46, 47). In one particular case, it has been confirmed that biodegradable MNPs may pose a more severe ecological risk than nonbiodegradable ones (e.g., PE) (17). On the other hand, and importantly, among all these MNPs, PLA or PLGA provides the currently most technically sound platform for encapsulating DNA fragments, rendering it more suitable than polymers such as PE and PS for constructing internally DNA-labeled MNPs (26, 40). This is because PLA or PLGA can be processed using a well-established emulsion-based preparation method, which allows the production of spherical MNPs with tunable particle sizes. This feature was essential for comparing the size-dependent uptake and translocation behavior of 200 and 700 nm MNPs in lettuce. In contrast, MNPs such as PS and PE cannot yet achieve effective labeling of DNA fragments through the emulsion-based preparation method.

Our findings further supported the important role of transpiration in facilitating the uptake and translocation of MNPs in lettuce. Under elevated transpiration tension, both root uptake and upward transport of MNPs to aerial tissues were significantly enhanced. The BCF reached up to 1.1×10^{-4} and the TF peaked at 38.2 during the initial exposure stage. These results offer further quantitative evidence, corroborating the fluorescence-based findings reported by Li et al., who pinpointed transpiration as a primary force governing the transport of MNP within plants (18). Consistent with the classical cohesion-tension theory, which describes water transport driven by transpirational pull in xylem vessels (23, 48), we propose that MNPs are primarily transported via water pathways—specifically the apoplastic route and xylem vessels. Enhanced transpiration accelerates water flow, thereby facilitating MNP transport throughout plant tissues. These findings further support the tight coupling between water dynamics and MNP translocation (49, 50).

Particle size also emerged as an important factor influencing the uptake and translocation of MNPs in lettuce. The 200 nm particles were absorbed more efficiently (BCF = 1.5×10^{-2}) and were rapidly translocated to leaves. In contrast, the 700 nm particles showed lower uptake (BCF = 1.9×10^{-4}) and remained largely retained in the roots. Kinetic analysis indicated continuous accumulation of the small MNPs in the leaves throughout the exposure period, whereas the large MNPs, despite some initial translocation, accumulated mainly in the roots over time. These findings are consistent with earlier reports indicating a strong size-dependent absorption pattern (18), in which 0.2 μm polystyrene particles are effectively absorbed and translocated to stems and leaves, and 2 μm particles are primarily restricted to the roots with reduced efficiency. Notably, a similar trend was observed by Li et al. (51), who found that 0.2 μm polystyrene particles were absorbed by maize seedlings at rates 1.7-, 1.9-, and 8.2-fold higher than those of 0.5, 1, and 2 μm particles, respectively. This size-dependent differential uptake can be further attributed to the plant's inherent structural features. Specifically, root features, such as lateral root development, cell wall composition, and Casparian strip integrity, collectively form a selective barrier system that governs the observed size-dependent uptake patterns (21, 52, 53).

Downloaded from https://www.pnas.org by CHINA AGRICULTURAL UNIVERSITY on August 27, 2026 from IP address 202.112.160.48.

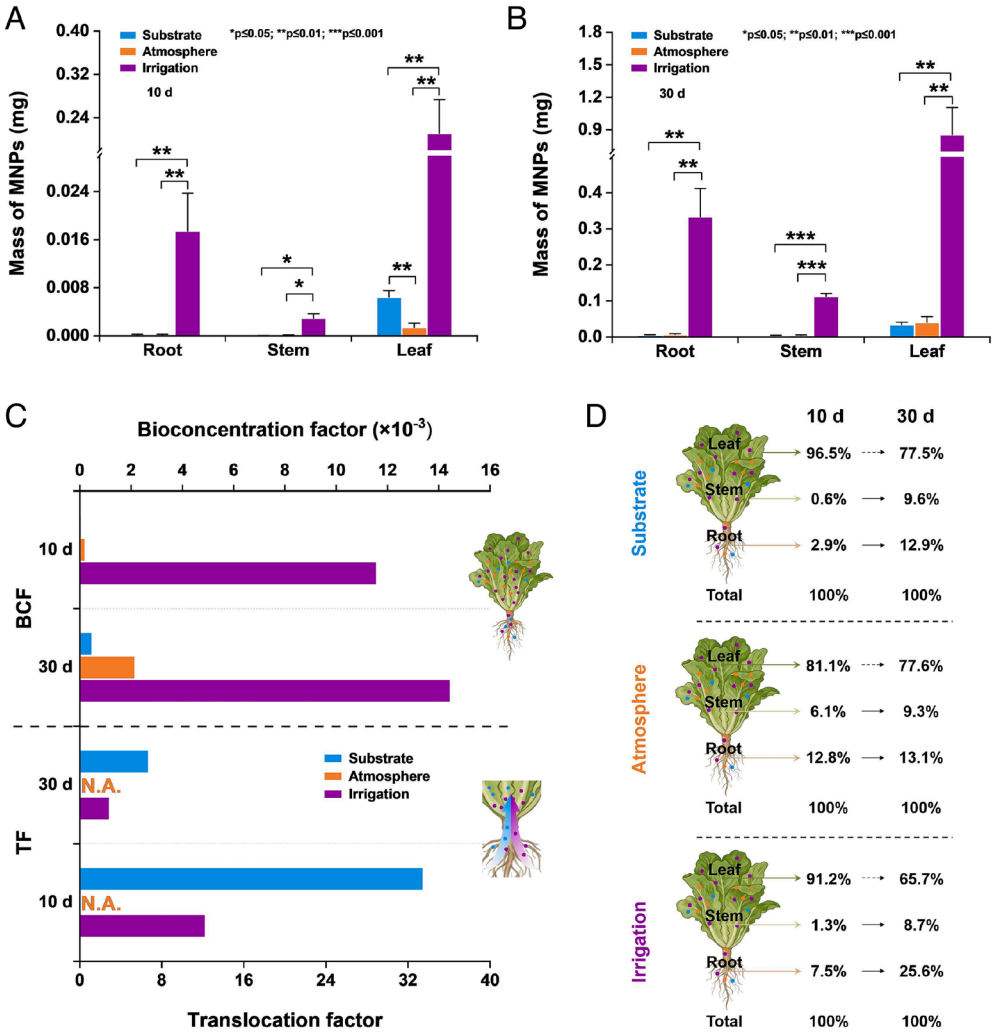

Fig. 6. Source-dependent uptake, translocation, and distribution of MNPs in lettuce. Net MNP accumulation in lettuce roots, stems, and leaves under three exposure pathways (substrate, atmosphere, and irrigation) at (*A*) day 10 and (*B*) day 30. (*C*) BCF (the ratio of MNP mass in whole lettuce seedlings to the initial MNP mass of the exposure medium) and TF (the ratio of MNP mass in aerial tissues to root tissues) for the different MNP exposure sources on days 10 and 30. Note that TF values were not calculated for the atmosphere group, as MNPs primarily enter lettuce via direct foliar uptake rather than root-to-shoot translocation. (*D*) Temporal variations in the relative MNP distribution proportions (%) in lettuce tissues across the three exposure pathways. Solid and dashed arrows indicate increased and decreased MNP proportional distribution, respectively. Error bars indicate SD, and data are shown as mean ± SD based on three independent biological replicates ($n = 3$). Significant differences between exposure pathways were determined using independent-samples *t* tests ($n = 3$). *$P \le 0.05$; **$P \le 0.01$; ***$P \le 0.001$. N.A. indicates not applicable.

The exposure pathway critically influences MNP bioaccumulation in lettuce. Irrigation represents the most bioavailable source, exhibiting a BCF of 1.5×10^{-2}, substantially higher than those for atmosphere (2.2×10^{-3}) and substrate (4.9×10^{-4}). This high bioavailability is attributed to prolonged root contact and transpiration-driven transport, which continuously facilitates particle uptake into lettuce biomass (50). In contrast, MNPs in the substrate were largely immobilized by soil adsorption and filtration, reducing pore water mobility and subsequent root contact, thereby lowering bioavailability (54–57). Nevertheless, consistent with prior report (22), we observed significantly higher translocation efficiency of MNPs from the substrate. This aligns with other root-exposure pathways (e.g., hydroponics and irrigation), where early-stage, low-accumulation translocation to the leaves results in a high TF. At lower accumulation levels, transpiration pull effectively drives limited internalized MNPs directly to the canopy; conversely, higher uptake leads to a greater retention in the roots and stems, with less continuous transport to the leaves. This temporal variation indicates dynamic tissue distribution of internalized MNPs during prolonged exposure. Supporting evidence shows nanoplastics accumulate in various plant tissues rather than a single organ, with distribution patterns varying across tissues and plant species (58). In addition, this study provides further quantitative evidence that leaf stomata serve as a major entry route for MNPs into plant tissues, supporting the findings of Li et al. (23), who previously identified stomata as critical entry points for MNPs. It is noteworthy that, regardless of the transpiration rate, particle size, or MNP source, both the accumulation and BCF of MNPs in lettuce increased significantly with exposure time. This indicates the continuous accumulation capacity of plants for MNPs and highlights the nonnegligible risks associated with long-term exposure.

While this study successfully utilized synthetic DNA tracer technology to elucidate the uptake patterns of MNPs by plants, the present work was limited to biodegradable PLGA MNPs. Considering that both polymer type and particle shape can influence the uptake and translocation of MNPs in plants, future research is warranted to validate the applicability of this synthetic

Downloaded from https://www.pnas.org by CHINA AGRICULTURAL UNIVERSITY on August 27, 2026 from IP address 202.112.160.48.

DNA tracing approach to more environmentally relevant MNPs, including nonbiodegradable polymers (e.g., PE, PS, and PMMA) and commonly observed morphologies (e.g., fibers and fragments). Effective encapsulation of synthetic DNA within these polymers will be a critical research priority, as well-established emulsion-based methods have not yet been demonstrated to be feasible. Novel approaches may therefore be required to achieve internal encapsulation while enabling precise control over particle size and shape.

Another concern is that, despite the excellent repeatability and high coefficient of linear correlation ($R^2 > 0.98$) of the established MNP concentration-qPCR Cq value calibration curve, its DNA amplification efficiency is suboptimal. For valid qPCR quantification, the DNA amplification efficiency of a standard calibration curve is ideally required to fall within the range of 90 to 110% (59, 60). Nevertheless, the DNA amplification efficiencies in this study deviate from this optimal range, which are primarily associated with the DNA encapsulation technique employed herein. In this study, DNA fragments were encapsulated in PLGA MNPs to establish a calibration curve correlating MNP concentrations with qPCR Cq values, which differs from the conventional qPCR standard curve that reflects the ideal relationship between pure DNA concentrations and qPCR Cq values. In this quantification system, DNA serves merely as an intermediate conversion indicator. Notably, the encapsulated DNA fragments need to be released from PLGA MNPs prior to qPCR amplification. As a result, the DNA Cq values are not exclusively governed by the qPCR amplification process. A variety of interfering factors jointly affect the final qPCR signals, including MNP dispersion status, heterogeneous DNA encapsulation, inconsistent DNA release efficiency from MNPs, and particle loss during dilution (40, 61). In addition, residual PCR inhibitors generated during MNP fabrication and DNA extraction, together with the inherent variability in amplification efficiency of different DNA sequences (31, 62, 63), further contribute to the unsatisfactory amplification efficiency. In line with the present results, previous studies adopting analogous encapsulation strategies using materials such as PLA, PLGA, and silica have also reported nonideal amplification efficiency of the constructed qPCR calibration curves (64, 65). Accordingly, future work will focus on improving the uniformity of DNA encapsulation and extraction, designing, and screening DNA sequences with consistent amplification efficiency to eliminate the inherent variability among different fragments. These improvements are expected to optimize the DNA amplification efficiency for PLGA encapsulation system and further improve the reliability of MNP mass quantification based on qPCR signal conversion.

3. Conclusion

This study established and validated an approach combining synthetic DNA labeling technology with qPCR detection to quantitatively investigate the uptake of PLGA MNPs in plants. This approach addresses the drawbacks of conventional labeling techniques, which fail to differentiate MNPs from distinct sources or with varying particle sizes. The results provide quantitative evidence that elevated transpiration enhances the MNP uptake and translocation, and that smaller MNPs are more efficiently absorbed and transported than larger counterparts. Lettuce exhibited the highest MNP uptake efficiently from irrigation water, driven by sustained root exposure. In comparison, atmospheric MNPs primarily penetrated plant tissues through stomata, while substrate MNPs showed limited bioavailable due to soil adsorption and immobilization. Leveraging the unique advantages of the synthetic DNA labeling technology, such as molecular programmability and high detection sensitivity, this study achieved high-resolution characterization of the uptake dynamics of coexisting MNPs with varied sources and sizes under complex environmental conditions. The established methodology offers a powerful tool for tracking environmental MNP pollution, assessing ecological risks, and ensuring agricultural food safety.

4. Materials and Methods

4.1. Fabricating and Characterizing DNA-Labeled MNPs. We employed PLGA (50:50; Jinan Daigang Bioengineering Co., Ltd) as experimental MNPs. 80-nucleotide single-stranded DNA (ssDNA) fragments, synthesized by Genewiz (Beijing, China), were utilized to label the MNP particles. These DNA sequences were adopted from one prior literature report (66). Full details of the DNA and primer sequences are provided in *SI Appendix*, Table S3.

DNA-labeled PLGA (DNA-PLGA) MNPs were fabricated using the double-emulsion ($W_1/O/W_2$) method (Fig. 1*A*) (40). Briefly, the primary water-in-oil (W_1/O) emulsion was formed by homogenizing the aqueous DNA solution (W_1 phase) with organic PLGA solution (O phase). This resultant W_1/O emulsion was then dispersed into a secondary aqueous phase (W_2) containing vitamin E-TPGS to form a complete double emulsion. After solvent evaporation and particle solidification, the products were repeatedly washed and purified to yield the final DNA-PLGA particles. Control PLGA particles were prepared following an identical protocol, with the sole omission of DNA in the initial aqueous phase. Full experimental procedures are described in *SI Appendix*, Text S1.

Fourier-transform infrared spectroscopy (FTIR, Nicolet 470 FTIR, Thermo Scientific) was used to characterize the surface functional groups of DNA-free and DNA-PLGA particles. Prior to analysis, the particle suspensions were freeze-dried to obtain dry powder samples. The dried samples were pressed into KBr pellets for FTIR measurement, and spectra were collected at room temperature over the wavenumber range of 400 to 4,000 cm^{-1}. Each spectrum was recorded with 32 scans at a spectral resolution of 4 cm^{-1}. Particle morphology was visualized using SEM (SU8010, Hitachi, JPN) at an accelerating voltage of 5 kV. A nanoparticle size analyzer (BeNano 90 Zeta, Dandong Baite) was used to determine the hydrodynamic size distribution and zeta potential at a particle concentration of 100 mg L^{-1}.

To establish a robust quantification strategy, we first verified the specificity of five synthetic DNA sequences and their matched primer pairs, followed by calibration of the qPCR signal against the concentration of DNA-PLGA MNPs. For primer-specificity validation, each synthetic DNA sequence (10^{-3} μM) was amplified with its matched primer pair, as well as the primer pairs corresponding to the remaining four DNA sequences. The PCR products were subsequently analyzed by agarose gel electrophoresis to confirm that each DNA sequence was specifically amplified only by its matched primer pair, without nonspecific amplification by the other mismatched primer pairs. The detailed compositions of the PCR reaction system and amplification protocols are provided in *SI Appendix*, Text S2. Subsequently, to establish a quantitative correlation between qPCR signals and MNP concentration, a stock suspension containing 50 mg of DNA-PLGA MNPs in 10 mL of distilled water was prepared via sonication and serially diluted. DNA was extracted from these samples using dichloromethane (40) (as described in *SI Appendix*, Text S3). Calibration curves were generated by plotting the measured Cq values against the known concentrations of DNA-PLGA MNPs. For each of the five DNA-PLGA MNP types, three independent replicate calibration curves were established, and each concentration point within each independent replicate was measured with three technical replicates. Detailed qPCR protocols are available in *SI Appendix*, Text S4.

To evaluate the efficiency of DNA encapsulation and extraction for DNA-PLGA MNPs, two quantitative indices were introduced: encapsulation efficiency and extraction efficiency (40). Detailed calculation procedures are described in *SI Appendix*, Text S5. The stability of DNA-PLGA MNPs in 1/5-strength Hoagland solution was further assessed using blank control and treatment groups. Samples were collected after 1, 2, 4, and 6 d of continuous agitation to quantify DNA leakage.

Downloaded from https://www.pnas.org by CHINA AGRICULTURAL UNIVERSITY on August 27, 2026 from IP address 202.112.160.48.

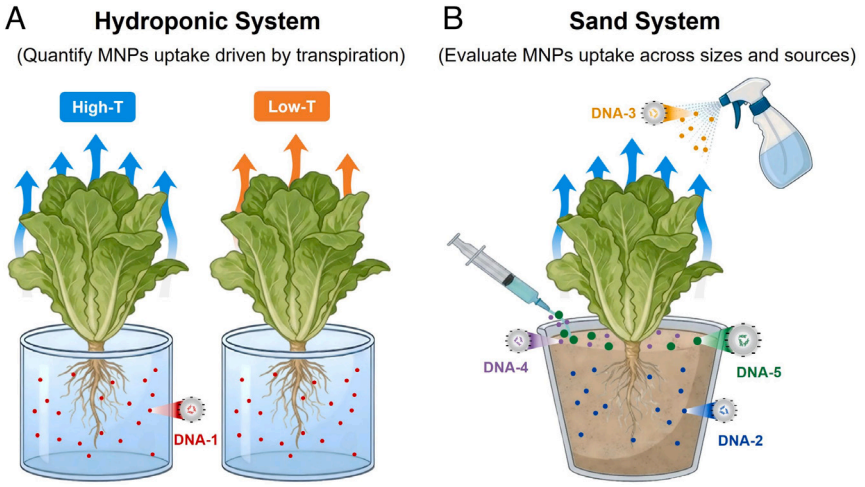

Fig. 7. Experimental schematic diagrams of MNP uptake assays in lettuce. (*A*) Hydroponic cultivation experiments for investigating the effects of transpiration pull on MNP uptake; 200 nm MNPs labeled with the DNA-1 sequence were used. (*B*) River sand cultivation experiments for exploring size-dependent and source-dependent MNP uptake; substrate-, atmosphere-, and irrigation-derived MNPs were respectively represented by 200 nm particles labeled with DNA-2, 200 nm particles labeled with DNA-3, and a mixture of 200 nm (DNA-4) and 700 nm (DNA-5) particles.

4.2. Lettuce Cultivation Experiments.

4.2.1. Hydroponic system. Lettuce (*L. sativa* L.) served as the experimental plant in this study. Hydroponic cultivation was performed to explore the uptake, translocation, and in-plant distribution of MNPs under varied transpiration conditions. These experiments were carried out inside a programmable growth chamber (BIC-300, BOXUN, China) to maintain stable temperature and humidity conditions (*SI Appendix*, Fig. S4). To eliminate unintended background contamination from environmental MNPs, all hydroponic experiments were conducted in a sealed growth chamber that was thoroughly cleaned prior to plant cultivation. All glassware and cultivation vessels were rinsed extensively with filtered distilled (DI) water before use. The DI water was prepurified via vacuum filtration through a 0.25 μm membrane, and all cultivation nutrient solutions were prepared using this filtered water (67). To minimize airborne particle deposition during cultivation, all handling of culture vessels was kept brief. Meanwhile, blank control groups without DNA-PLGA MNP exposure were established and processed following the same cultivation, extraction, DNA release, and qPCR procedures as the treatment groups. Since the qPCR assay exclusively targets and amplifies the synthetic DNA sequences encapsulated within the MNPs, environmental background plastics without these specific DNA sequences yield no positive signals. These stringent experimental measures therefore minimized exogenous MNP introduction and prevented associated biases in MNP quantification. Lettuce seed pretreatment was performed in accordance with Li et al. (18), with the full experimental procedures are provided in *SI Appendix*, Text S6.

To evaluate the effect of plant transpiration on MNP uptake, vapor pressure deficit (VPD) was manipulated to establish differential transpiration levels. Both high- and low-transpiration treatments were maintained under a 16-h light/8-h dark photoperiod, with a daytime light intensity of 13,888 lx and a nighttime temperatures of 20 °C. During the light period, the high-transpiration condition was set at 30 °C and 50% relative humidity (RH), generating a high VPD of 2.12 kPa. In contrast, the low-transpiration condition was maintained at 15 °C and 80% RH, yielding a low VPD of 0.34 kPa to suppress transpiration (Fig. 7*A*). This experimental design allowed a direct comparison of MNP uptake under two distinct scenarios. VPD values were calculated based on ambient temperature (T) and RH (18, 68):

$$VPD = 0.61078 \times e^{\frac{17.27 \times T}{237.3 + T}} \times (1 - RH), \quad [1]$$

where *VPD* is the vapor pressure deficit (kPa), *T* is the ambient temperature (°C), and *RH* is the ambient relative humidity (%).

4.2.2. River sand system. River sand was adopted as the cultivation substrate to investigate the differential uptake of MNPs by lettuce from three environmental sources (substrate, atmosphere, and irrigation) and two particle sizes (approximately 200 and 700 nm) (Fig. 7*B* and *SI Appendix*, Fig. S5). Seed germination and seedling cultivation were performed following the same hydroponic protocol described above. Temperature and humidity were controlled using the same growth chamber utilized for hydroponic cultivation. To eliminate potential background contamination and reduce airborne particle deposition, we thoroughly cleaned river sand, culture vessels, and experimental tools before use, minimized vessel handling time, and prepared all irrigation and wet-deposition solutions with filtered DI water (67).

Blank control and treatment groups were both established. The substrate of the treatment group was premixed with DNA-PLGA MNPs (150 mg kg^{-1}) to simulate soil residual MNPs before transplantation (18). Following transplantation, lettuce seedlings were irrigated and subjected to wet-depositions (atmosphere) every 2 d. The irrigation and wet-deposition solutions for the treatment group contained 50 mg L^{-1} DNA-PLGA MNPs (18), while the blank control group received equivalent volumes of filtered DI water. To further assess the size-dependent uptake of MNPs, the irrigation solutions for the treatment group were supplemented with MNPs of two particle sizes (approximately 200 and 700 nm). Control groups were processed in parallel through the same extraction, DNA release, and qPCR quantification procedures to quantify background signals. Lettuce seedlings were grown under a 16-h light/8-h dark photoperiod, with a daytime temperatures of 30 °C, a nighttime temperatures of 20 °C, 50% RH, and a light intensity of 13,888 lx, generating a VPD of 2.12 kPa. Full procedural details are provided in *SI Appendix*, Text S7.

4.3. Extraction of DNA-Labeled MNPs from Lettuce.

Lettuce seedlings were sampled on days 10 and 30 after transplantation. The sampled tissues were sequentially washed, cut, freeze-dried, and ground into powder. Detailed pretreatment protocols are provided in *SI Appendix*, Text S8. MNP extraction from lettuce tissues was performed following a modified protocol from Li et al. (20). The extraction procedure involved four main steps: alkaline digestion, cellulose precipitation, resuspension, and filtration. Specifically, 15 mg of homogenized plant powder was mixed with 0.9 mL tetramethylammonium hydroxide (TMAH) solution, and the mixture was then shaken at 1,000 rpm for 24 h to achieve complete tissue digestion. The digestate was washed four times with 3 mL absolute ethanol per cycle to remove residual TMAH and precipitate cellulose. Following the final centrifugation, the supernatant was discarded, and the resulting pellet was air-dried in a fume hood for 2 h to evaporate residual ethanol. The dried precipitate was resuspended in 1 mL of distilled water, uniformly dispersed by ultrasonication, and filtered through sized-matched filter paper to recover DNA-PLGA MNP particles (Fig. 8). This extraction process was performed independently for lettuce root, stem, and leaf tissues.

4.4. Analysis of MNP Uptake and Translocation.

4.4.1. Quantification of MNP uptake and translocation. Subsequent to DNA-PLGA MNP extraction, the encapsulated DNA fragments within these MNPs were released using dichloromethane, followed by qPCR quantification (40). The MNP concentration was calculated according to a preestablished linear

Downloaded from https://www.pnas.org by CHINA AGRICULTURAL UNIVERSITY on August 27, 2026 from IP address 202.112.160.48.

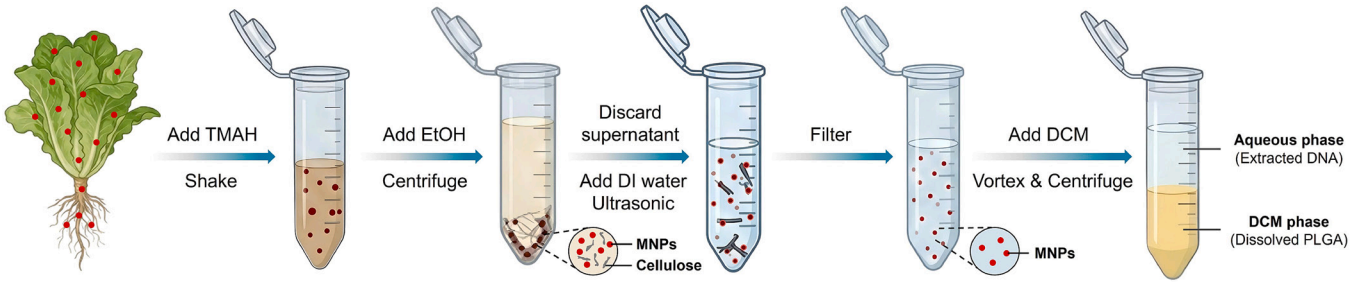

Fig. 8. Schematic illustration of the experimental workflow for extracting DNA-PLGA MNPs from lettuce tissues and releasing their encapsulated DNA fragments from DNA-PLGA MNPs.

correlation between DNA signal intensity and MNP concentration. To guarantee quantification accuracy, rigorous background correction and threshold calibration were performed. The method detection limit (MDL) was defined as the minimum MNP concentration that can be reliably quantified within the linear range of the standard curve. The net MNP concentration in lettuce tissues was calculated by subtracting the mean background value of the control group from the measured values of the treatment group. These background-corrected values were further compared against the MDL. Signals below the MDL were defined as nondetectable and assigned a value of zero, while only those exceeding the MDL were regarded as positive uptake (26). Ultimately, the total MNP accumulation in individual lettuce tissues (roots, stems, and leaves) was calculated by multiplying the validated net concentration by the corresponding tissue biomass. To evaluate the uptake and translocation capabilities of lettuce for MNPs, two typical indices were adopted: the bioconcentration factor (BCF) and the translocation factor (TF). The BCF reflects the lettuce's ability to absorb MNPs from environmental matrices (69):

$$BCF = \frac{MNP_{entire\ plant}}{MNP_{exposure\ medium}}, \quad [2]$$

where $MNP_{entire\ plant}$ is the MNP mass detected in the entire plant, and $MNP_{exposure\ medium}$ is the initial MNP mass applied to the exposure medium. The TF indicates the efficiency of MNP translocation from roots to aerial tissues (stems and leaves) (70):

$$TF = \frac{MNP_{aerial\ tissues}}{MNP_{roots}}, \quad [3]$$

where $MNP_{aerial\ tissues}$ is the MNP mass detected in the aerial tissues, and MNP_{roots} is the MNP mass retained in the roots.

4.4.2. Statistical analysis. All statistical analyses were performed using IBM SPSS Statistics (version 27.0). All data are presented as the mean ± SD of three independent biological replicates. For lettuce uptake experiments, each biological replicate corresponded to an individually cultivated lettuce seedling grown in a separate culture vessel. Differences between the two groups were analyzed using independent-samples *t* tests. One-way ANOVA was used for multigroup comparisons to evaluate the effects of different preparation conditions on the particle sizes and Zeta potential of DNA-PLGA MNPs. Post hoc multiple comparisons were further performed using the LSD or Duncan's multiple range test where applicable. Levene's test was adopted to verify variance homogeneity, and the statistical methods were selected in accordance with the variance assumption. Statistical significance was set at $P \leq 0.05$. In the figures, error bars represent SD, and asterisks denote significant differences between groups: $*P \leq 0.05$; $**P \leq 0.01$; $***P \leq 0.001$. "ND" refers to nondetectable.

Data, Materials, and Software Availability. All study data are included in the article and/or *SI Appendix*.

ACKNOWLEDGMENTS. This work was supported by the National Natural Science Foundation of China (42477317).

Author affiliations: [a]Department of Land Engineering, College of Land Science and Technology, State Key Laboratory of Efficient Utilization of Agricultural Water Resources, Key Laboratory of Arable Land Conservation in North China, Ministry of Agriculture and Rural Affairs, China Agricultural University Beijing 100193, People's Republic of China; [b]Department of Hydraulic Engineering, College of Water Resources and Civil Engineering, State Key Laboratory of Efficient Utilization of Agricultural Water Resources, China Agricultural University, Beijing 100083, People's Republic of China; [c]Department of Chemistry, State Key Laboratory of Molecular Engineering of Polymers, Shanghai Key Laboratory of Molecular Catalysis and Innovative Materials, College of Chemistry and Materials, Fudan University, Shanghai 200438, People's Republic of China; [d]Department of Environmental Sciences, University of California Riverside, Riverside, CA 92521; and [e]Department of Biological & Environmental Engineering, Cornell University, New York, NY 14853

Author contributions: R.L. designed research; Z.D., C.W., Y.L., and X.L. performed research; Z.D., R.L., C.S., Y.X., D.Y., J.Š., and D.L. contributed new reagents/analytic tools; Z.D., C.W., R.L., Y.L., X.L., C.S., and Y.X. analyzed data; and Z.D., C.W., R.L., D.Y., J.Š., and D.L. wrote the paper.

1. R. Geyer, J. R. Jambeck, K. L. Law, Production, use, and fate of all plastics ever made. *Sci Adv.* **3**, e1700782 (2017).
2. A. L. Andrady, M. A. Neal, Applications and societal benefits of plastics. *Philos. Trans. R. Soc. Lond. B, Biol. Sci.* **364**, 1977–1984 (2009).
3. A. Kukkola, A. J. Chetwynd, S. Krause, I. Lynch, Beyond microbeads: Examining the role of cosmetics in microplastic pollution and spotlighting unanswered questions. *J. Hazard Mater.* **476**, 135053 (2024).
4. H. Wallace, Presence of microplastics and nanoplastics in food, with particular focus on seafood. *EFSA J.* **14**, e04501 (2016).
5. R. C. Thompson *et al.*, Lost at sea: Where is all the plastic? *Science* **304**, 838–838 (2004).
6. J. P. G. L. Frias, R. Nash, Microplastics: Finding a consensus on the definition. *Mar. Pollut. Bull.* **138**, 145–147 (2019).
7. E.-L. Ng *et al.*, An overview of microplastic and nanoplastic pollution in agroecosystems. *Sci. Total Environ.* **627**, 1377–1388 (2018).
8. L. Nizzetto, M. Futter, S. Langaas, Are agricultural soils dumps for microplastics of urban origin? *Environ. Sci. Technol.* **50**, 10777–10779 (2016).
9. X. F. Jiang *et al.*, Ecotoxicity and genotoxicity of polystyrene microplastics on higher plant *Vicia faba*. *Environ. Pollut.* **250**, 831–838 (2019).
10. M. Zocchi, R. Sommaruga, Microplastics modify the toxicity of glyphosate on *Daphnia magna*. *Sci. Total Environ.* **697**, 134194 (2019).
11. Y. Mato *et al.*, Plastic resin pellets as a transport medium for toxic chemicals in the marine environment. *Environ. Sci. Technol.* **35**, 318–324 (2001).
12. D. Boyle, A. I. Catarino, N. J. Clark, T. B. Henry, Polyvinyl chloride (PVC) plastic fragments release Pb additives that are bioavailable in zebrafish. *Environ. Pollut.* **263**, 114422 (2020).
13. X. Li *et al.*, PMMA nanoplastics induce gastric epithelial cellular senescence and cGAS-STING-mediated inflammation via ROS overproduction and NHEJ suppression. *Ecotox. Environ. Saf.* **287**, 117284 (2024).
14. J. Yang, G. Smagghe, X. M. Wu, W. P. Zhang, X. S. Chen, Divergent impacts of conventional and biodegradable microplastics on pesticide fate and toxicity in a soil-chive system, underscoring a soil-plant-microbe disruption. *Pestic. Biochem. Physiol.* **218**, 106971 (2026).
15. B. G. Lin *et al.*, From biodegradation to biohazard: Polylactic acid microplastics induced rice growth inhibition in agroecosystems. *J. Hazard Mater.* **496**, 139420 (2025).
16. W. Q. Xu, Y. S. Liu, M. Hu, H. Y. Yu, L. J. Bao, Impact of microplastics on microbial communities and arsenic speciation transformation at arsenic-contaminated soil. *J. Instrum. Anal.* **43**, 1220–1226 (2024).
17. M. Qin *et al.*, The role of microplastics in altering arsenic fractionation and microbial community structures in arsenic-contaminated riverine sediments. *J. Hazard Mater.* **433**, 128801 (2022).
18. L. Z. Li *et al.*, Effective uptake of submicrometre plastics by crop plants via a crack-entry mode. *Nat. Sustain.* **3**, 929–937 (2020).
19. X. D. Sun *et al.*, Differentially charged nanoplastics demonstrate distinct accumulation in *Arabidopsis thaliana*. *Nat. Nanotechnol.* **15**, 755–762 (2020).
20. C. J. Li *et al.*, Quantification of nanoplastic uptake in cucumber plants by pyrolysis gas chromatography/mass spectrometry. *Environ. Sci. Technol. Lett.* **8**, 633–638 (2021).
21. J. H. Zhu, J. Wang, R. N. Chen, Q. R. Feng, X. H. Zhan, Cellular process of polystyrene nanoparticles entry into wheat roots. *Environ. Sci. Technol.* **56**, 6436–6444 (2022).
22. Y. M. Luo *et al.*, Quantitative tracing of uptake and transport of submicrometre plastics in crop plants using lanthanide chelates as a dual-functional tracer. *Nat. Nanotechnol.* **17**, 424–431 (2022).
23. Y. Li *et al.*, Leaf absorption contributes to accumulation of microplastics in plants. *Nature* **641**, 666–673 (2025).

Downloaded from https://www.pnas.org by CHINA AGRICULTURAL UNIVERSITY on August 27, 2026 from IP address 202.112.160.48.

24. B. J. Mahler, M. Winkler, P. Bennett, D. M. Hillis, DNA-labeled clay: A sensitive new method for tracing particle transport. *Geology* **26**, 831–834 (1998).
25. D. Paunescu, M. Puddu, J. O. B. Soellner, P. R. Stoessel, R. N. Grass, Reversible DNA encapsulation in silica to produce ROS-resistant and heat-resistant synthetic DNA "fossils". *Nat. Protoc.* **8**, 2440–2448 (2013).
26. H. E. Dahlke *et al.*, Using concurrent DNA tracer injections to infer glacial flow pathways. *Hydrol. Process.* **29**, 5257–5274 (2015).
27. M. Puddu, D. Paunescu, W. J. Stark, R. N. Grass, Magnetically recoverable, thermostable, hydrophobic DNA/silica encapsulates and their application as invisible oil tags. *ACS Nano.* **8**, 2677–2685 (2014).
28. R. K. Liao, P. L. Yang, W. Y. Wu, D. Luo, D. Y. Yang, A DNA tracer system for hydrological environment investigations. *Environ. Sci. Technol.* **52**, 1695–1703 (2018).
29. C. X. Wang, D. Y. Yang, D. Luo, R. K. Liao, The appication of DNA nanotechnology to trace water environmental pollution. *Chin. Sci. Bull.* **69**, 112–126 (2024).
30. R. K. Liao, J. J. Zhang, T. T. Li, D. Luo, D. Y. Yang, Biopolymer/plasmid DNA microspheres as tracers for multiplexed hydrological investigation. *Chem. Eng. J.* **401**, 126035 (2020).
31. A. N. Sharma, D. Luo, M. T. Walter, Hydrological tracers using nanobiotechnology: Proof of concept. *Environ. Sci. Technol.* **46**, 8928–8936 (2012).
32. C. B. Georgakakos, P. L. Richards, M. T. Walter, Tracing septic pollution sources using synthetic DNA tracers: Proof of concept. *Air Soil Water Res.* **12**, 1–7 (2019).
33. C. A. Mora *et al.*, Ultrasensitive quantification of pesticide contamination and drift using silica particles with encapsulated DNA. *Environ. Sci. Technol. Lett.* **3**, 19–23 (2016).
34. C. X. Wang, Z. F. Duan, R. K. Liao, J. Simunek, D. Luo, High-resolution characterization of the size exclusion effect on the transport of low-concentration mixed-size colloids in porous media using a synthetic DNA-labeling method. *Environ. Sci. Technol.* **59**, 12232–12243 (2025).
35. S. Galindo-Rodriguez, E. Allémann, H. Fessi, E. Doelker, Physicochemical parameters associated with nanoparticle formation in the salting-out, emulsification-diffusion, and nanoprecipitation methods. *Pharm. Res.* **21**, 1428–1439 (2004).
36. S. K. Sahoo, J. Panyam, S. Prabha, V. Labhasetwar, Residual polyvinyl alcohol associated with poly (d, l-lactide-co-glycolide) nanoparticles affects their physical properties and cellular uptake. *J. Control. Release* **82**, 105–114 (2002).
37. T. S. H. Leong, T. J. Wooster, S. E. Kentish, M. Ashokkumar, Minimising oil droplet size using ultrasonic emulsification. *Ultrason. Sonochem.* **16**, 721–727 (2009).
38. S. M. Jafari, Y. He, B. Bhandari, Production of sub-micron emulsions by ultrasound and microfluidization techniques. *J. Food Eng.* **82**, 478–488 (2007).
39. N. Anton, J.-P. Benoit, P. Saulnier, Design and production of nanoparticles formulated from nano-emulsion templates–A review. *J. Control. Release* **128**, 185–199 (2008).
40. C. P. McNew, C. Z. Wang, M. T. Walter, H. E. Dahlke, Fabrication, detection, and analysis of DNA-labeled PLGA particles for environmental transport studies. *J. Colloid Interface Sci.* **526**, 207–219 (2018).
41. F. He, J. Q. Fu, R. Wang, Synthesis and structural properties of polylactic acid/polyglycolic acid copolymer. *China Synth. Fiber Ind.* **39**, 42–44 (2016).
42. B. B. Chen *et al.*, Investigation of the thermal stability and hydrolytic degradation kinetics of poly(lactide-co-glycolide) melts. *AAPS PharmSciTech* **26**, 24 (2025).
43. B. Maryam, M. Asim, J. X. Li, H. Qayyum, X. H. Liu, Luminous polystyrene upconverted nanoparticles to visualize the traces of nanoplastics in a vegetable plant. *Environ. Sci. Nano* **12**, 1273–1287 (2025).
44. Y. X. Feng, W. Q. Hua, J. Lu, J. Wu, C. Zhang, Adsorption and desorption of nonylphenol on the biodegradable microplastics in seawater. *J. Clean. Prod.* **476**, 143778 (2024).
45. M. N. Allemann *et al.*, Rapid biodegradation of microplastics generated from bio-based thermoplastic polyurethane. *Sci. Rep.* **14**, 6036 (2024).
46. F. Y. Wang, X. Q. Zhang, S. Q. Zhang, S. W. Zhang, Y. H. Sun, Interactions of microplastics and cadmium on plant growth and arbuscular mycorrhizal fungal communities in an agricultural soil. *Chemosphere* **254**, 126791 (2020).
47. Y. H. Lian *et al.*, Impact of polyethylene and polylactic acid microplastics on growth, physio-biochemistry and metabolism in soybean (*Glycine max*). *China Environ. Sci.* **42**, 2894–2903 (2022).
48. E. Steudle, J. Frensch, Water transport in plants: Role of the apoplast. *Plant Soil* **187**, 67–79 (1996).
49. J. P. Ding *et al.*, Effect of vapor pressure deficit on the photosynthesis, growth, and nutrient absorption of tomato seedlings. *Sci. Hortic.* **293**, 110736 (2022).
50. W. F. Wang *et al.*, Uptake, translocation, and biological impacts of micro(nano)plastics in terrestrial plants: Progress and prospects. *Environ. Res.* **203**, 111867 (2022).
51. H. B. Li *et al.*, Uptake and distribution of microplastics of different particle sizes in maize (*Zea mays*) seedling roots. *Chemosphere* **313**, 137491 (2023).
52. J. J. Yin *et al.*, Polystyrene nanoplastics induce cell type-dependent secondary wall reinforcement in rice (*Oryza sativa*) roots and reduce root hydraulic conductivity. *J. Hazard Mater.* **477**, 135309 (2024).
53. L. Y. Wang *et al.*, An unrecognized entry pathway of submicrometre plastics into crop root: The split of hole in protective layer. *J. Hazard Mater.* **457**, 131732 (2023).
54. M. Guo, R. Noori, S. Abolfathi, Microplastics in freshwater systems: Dynamic behaviour and transport processes. *Resour., Conserv. Recycl.* **205**, 107578 (2024).
55. K. Waldschläger, H. Schüttrumpf, Erosion behavior of different microplastic particles in comparison to natural sediments. *Environ. Sci. Technol.* **53**, 13219–13227 (2019).
56. Z. Y. Li *et al.*, The influence of aqueous iron on river sand's arsenic adsorption: Characteristics and mechanisms. *Water* **16**, 1107 (2024).
57. Y. N. Cao *et al.*, Effect and environmental behaviour of microplastics in soil. *Waste Manage. Res.* **42**, 511–519 (2023).
58. E. Zytowski, M. Mollavali, S. Baldermann, Uptake and translocation of nanoplastics in mono and dicot vegetables. *Plant, Cell Environ.* **48**, 134–148 (2025).
59. D. Svec, A. Tichopad, V. Novosadova, M. W. Pfaffl, M. Kubista, How good is a PCR efficiency estimate: Recommendations for precise and robust qPCR efficiency assessments. *Biomol. Detect. Quantif.* **3**, 9–16 (2015).
60. S. C. Taylor *et al.*, The ultimate qPCR experiment: Producing publication quality, reproducible data the first time. *Trends Biotechnol.* **37**, 761–774 (2019).
61. Y. Tang, J. W. Foppen, T. A. Bogaard, Transport of silica encapsulated DNA microparticles in controlled instantaneous injection open channel experiments. *J. Contam. Hydrol.* **242**, 103880 (2021).
62. T. C. Dingle, R. H. Sedlak, L. Cook, K. R. Jerome, Tolerance of droplet-digital PCR vs real-time quantitative PCR to inhibitory substances. *Clin. Chem.* **59**, 1670–1672 (2013).
63. M. Sidstedt, P. Rådström, J. Hedman, PCR inhibition in qPCR, dPCR and MPS–Mechanisms and solutions. *Anal. Bioanal. Chem.* **412**, 2009–2023 (2020).
64. X. Z. Kong *et al.*, Tomographic reservoir imaging with DNA-labeled silica nanotracers: The first field validation. *Environ. Sci. Technol.* **52**, 13681–13689 (2018).
65. Z. Li *et al.*, Tracing environmental DNA transport in a large lake with synthetic DNA microparticles and hydrodynamic modeling. *Environ. Sci. Technol.* **60**, 3519–3531 (2026).
66. J. W. Foppen, C. Orup, R. Adell, V. Poulalion, S. Uhlenbrook, Using multiple artificial DNA tracers in hydrology. *Hydrol. Process.* **25**, 3101–3106 (2011).
67. W. Cowger *et al.*, Reporting guidelines to increase the reproducibility and comparability of research on microplastics. *Appl. Spectrosc.* **74**, 1066–1077 (2020).
68. E. Wang, C. J. Smith, W. J. Bond, K. Verburg, Estimations of vapour pressure deficit and crop water demand in APSIM and their implications for prediction of crop yield, water use, and deep drainage. *Aust. J. Agric. Res.* **55**, 03216 (2004).
69. Z. Q. Wang *et al.*, Geochemical characteristics and health risk assessment of heavy metals in soil-crop systems. *Geophys. Geochem. Explor.* **49**, 943–953 (2025).
70. D. Chitimus *et al.*, Studies on the accumulation, translocation, and enrichment capacity of soils and the plant species *Phragmites australis* (common reed) with heavy metals. *Sustainability* **15**, su15118729 (2023).

Downloaded from https://www.pnas.org by CHINA AGRICULTURAL UNIVERSITY on August 27, 2026 from IP address 202.112.160.48.